Epsilon-near-zero enhancement of near-field radiative heat transfer in BP/hBN and BP/α-MoO_3 parallel-plate structures

Hodjat Hajian[1,*], Ivan D. Rukhlenko[2,3], Veysel Erçağlar[1,5], George Hanson[4], and Ekmel Ozbay[1,5,6,*]

[1] NANOTAM-Nanotechnology Research Center, Bilkent University, 06800 Ankara, Turkey
[2] The University of Sydney, School of Physics, Camperdown, 2006, NSW, Australia
[3] Information Optical Technologies Centre, ITMO University, Saint Petersburg, 197101, Russia
[4] Department of Electrical Engineering, University of Wisconsin, 3200 North Cramer Street, Milwaukee, WI, 53211, USA
[5] Department of Electrical and Electronics Engineering, Bilkent University, 06800, Ankara, Turkey
[6] Department of Physics and UNAM-Institute of Materials Science and Nanotechnology, Bilkent University, 06800 Ankara, Turkey

Authors to whom correspondence should be addressed: hodjat.hajian@bilkent.edu.tr, ozbay@bilkent.edu.tr

Abstract

Black phosphorous (BP) is a well-known two-dimensional van der Waals (vdW) material with in-plane anisotropy and remarkable electronic and optical properties. Here, we comprehensively analyze the near-field radiative heat transfer (NFRHT) between a pair of parallel non-rotated BP flakes that occurs due to the tunneling of the coupled anisotropic surface plasmon polaritons (SPPs) supported by the flakes. It is demonstrated that the covering of the BP flakes with hexagonal boron nitride (hBN) films leads to the hybridization of the BP's SPPs with the hBN's hyperbolic phonon polaritons (HPPs) and to the significant enhancement of the NFRHT at the hBN's epsilon-near-zero (ENZ) frequencies. It is also shown that the NFRHT in the BP/hBN parallel-plate structure can be actively switched between the ON and OFF states by changing the chemical potential of the BPs, and that the NFRHT can be modified by altering the number of the BP layers. Finally, we replace hBN with α-MoO_3 and explore how the NFRHT is spectrally and strongly modified in the BP/α-MoO_3 parallel-plate structure. We believe that the proposed BP/polar-vdW-material parallel-plate structures can prove useful in the thermal management of optoelectronic devices.

Keywords: Epsilon-near-zero materials; near-field radiative heat transfer; black phosphorous; hexagonal boron nitride; α-MoO_3

Following the pioneering work of Polder and Hove [1], the near-field radiative heat transfer (NFRHT) has attracted considerable attention in the last two decades due to its promising applications in thermophotovoltaics [2, 3], thermal rectification [4], electroluminescent cooling [5], thermal diodes [6], and transistors [7]. While the propagating waves contribute to the far-field radiative heat transfer [8], the evanescent waves are responsible for the heat flux in the NFRHT — also referred to as photon tunneling.

It is known that the NFRHT is considerably enhanced due the excitation of surface polaritons [9, 10]. The efficiency of the NFRHT can exceed the blackbody limit by several orders in magnitude *via* the resonant coupling of surface plasmon polaritons (SPPs) in structures based on metals [11, 12], doped Si [1-14], and surface phonon polaritons in heat transfer devices composed of SiO_2 [15], Al_2O_3 [16], and SiC [17, 18]. Moreover, it was shown that due to the thermal excitation of isotropic graphene SPPs, NFRHT between two closely spaced parallel-plates of graphene can be strongly mediated, enhanced, and tuned *via* the modification of the chemical potential of graphene in the infrared range [19-22].

Black phosphorous (BP) is often used as an anisotropic plasmonic van der Waals (vdW) material for the realization of enhanced NFRHT [23, 24]. It has a tunable bandgap, ranging from 1.51 eV for a monolayer BP to 0.59 eV for a five-layer BP, and a thickness-dependent anisotropic absorption coefficient [25]. The latter feature implies that, unlike graphene, the SPPs of BP exhibit anisotropic behavior [26]. Moreover, it has been reported that the thermal conductivities of BP along the zigzag and armchair directions are three orders of magnitude lower than that of graphene at 300 K [27]. This makes BP a better candidate than graphene for the heat management *via* NFRHT.

Recent studies have revealed that the NFRHT is greatly enhanced by the out-of-plane hyperbolic plasmon polaritons or phonon polaritons (HPPs) of metamaterials [28-32] as well as by the in-plane modes of the graphene-based [33, 34] or BP-based [35] metasurfaces. However, the dependence of the maximum wavenumber of HPPs on the size of the unit cell and the associated fabrication complexity (due to electron beam lithography or several film deposition processes) of the hyperbolic metamaterials or metasurfaces challenge their practical realization for the NFRHT purposes.

Naturally hyperbolic vdW materials such as hexagonal boron nitride (hBN) [36-38] and α-MoO_3 [39-40] have also been used to enhance the NFRHT. It has been demonstrated that the NFRHT can be mechanically tuned in twisted hBN films [37] or actively modulated in graphene-hBN heterostructures [41-43]. Because α-MoO_3 has different optical responses along its three crystallographic directions, a similar mechanical modulation of the NFRHT is observed for the twisted films of α-MoO_3 with differently aligned surfaces [40]. Despite a great deal of recent studies on this topic, the active modulation of enhanced NFRHT in non-rotated epsilon-near-zero BP/hBN and BP/α-MoO_3 parallel-plate structures has not been analyzed so far to the best of our knowledge.

In the present paper, we comprehensively analyze the NFRHT between two parallel non-rotated BP flakes covered with hBN films [Fig. 1(b)]. It is found that the coupling of the anisotropic plasmons of BP with the hyperbolic phonons of hBN considerably enhances the NFRHT near the edges of the Reststrahlen bands (RBs) of hBN, where hBN exhibits the epsilon-near-zero (ENZ) feature. We demonstrate the possibilities of the active and passive tunings of the NFRHT through changing the chemical potential and altering the number of layers of the BP flakes. It is also shown that the replacement of hBN with α-MoO_3 allows one to efficiently manipulate the spectrum of the NFRHT in the structure.

Figure 1(a) shows a schematic of two parallel and non-rotated N-layer BP flakes, which are separated by a vacuum gap of width d. The x and y axes denote the armchair (AC) and zigzag (ZZ) crystalline directions of the BP layers. In Fig. 1(b), the BP flakes are covered with hBN films so that their optical axes are aligned in the z direction. The top (emitter) and bottom (receiver) layers are kept at constant temperatures of $T_2 = 310\ \mathrm{K}$ and $T_1 = 290\ \mathrm{K}$. The NFRHT is characterized by the heat transfer coefficient (HTC), which measures the radiative heat conductance per unit area in the units of $\mathrm{W/(m^2K)}$ and is defined by the triple integral [10, 44]

$$h = \frac{q}{\Delta T} = \frac{1}{8\pi^3 \Delta T}\int_0^\infty [\Theta(\omega, T_2) - \Theta(\omega, T_1)]d\omega \iint_{-\infty}^{\infty} \xi(\omega, \beta_x, \beta_y) d\beta_x d\beta_y, \quad (1)$$

where q is net power per unit of area exchanged between the parallel plates, $\Theta(\omega, T_i) = \hbar\omega/[\exp(\hbar\omega/k_B T_i) - 1]$ is the mean energy of a Planck oscillator at angular frequency ω and temperature T_i, $\hbar$ is the reduced Planck's constant, $\Delta T = T_2 - T_1$, and k_B is the Boltzmann's constant. Moreover, for the case of $\Delta T \to 0$, $\frac{\Theta(\omega,T_2)-\Theta(\omega,T_1)}{\Delta T}$ should be replaced with $\frac{\partial\Theta(\omega,T)}{\partial T}$. The energy transmission coefficient or photon tunneling probability for propagating ($\beta < \beta_0$) and evanescent ($\beta > \beta_0$) modes is given by [10]

$$\xi(\omega, \beta_x, \beta_y) = \begin{cases} \mathrm{Tr}\left[(\mathbf{I} - \mathbf{R}_2^\dagger \mathbf{R}_2)\mathbf{D}_{12}(\mathbf{I} - \mathbf{R}_1 \mathbf{R}_1^\dagger)\mathbf{D}_{12}^\dagger\right], & \beta < \beta_0 \\ \mathrm{Tr}\left[(\mathbf{R}_2^\dagger - \mathbf{R}_2)\mathbf{D}_{12}(\mathbf{R}_1 - \mathbf{R}_1^\dagger)\mathbf{D}_{12}^\dagger\right]e^{-2|k_z|d}, & \beta > \beta_0 \end{cases} \quad (2)$$

where $\beta_0 = \omega/c$, $\beta = \sqrt{\beta_x^2 + \beta_y^2}$, and $k_z = \sqrt{\beta_0^2 - \beta^2}$ is the perpendicular wave vector component in vacuum. Here, the dagger denotes conjugate transpose, $\boldsymbol{I}$ is a 2×2 unit matrix, $\mathbf{D}_{12} = (\mathbf{I} - \mathbf{R}_1\mathbf{R}_2 e^{2ik_z d})^{-1}$, and

$$\mathbf{R}_{1,2} = \begin{pmatrix} r_{21,12}^{ss} & r_{21,12}^{sp} \\ r_{21,12}^{ps} & r_{21,12}^{pp} \end{pmatrix} \quad (3)$$

includes the Fresnel's reflections coefficients for the s- and p-polarized plane waves incident from the vacuum (medium 2) onto medium 1 and vice versa (see supplementary material for more details). The first and second letters of the superscript in each coefficient indicate the polarization states of the incident and the reflected waves, respectively.

In agreement with Ref. [45], the details of derivations, the permittivity of hBN, and the optical conductivity $\sigma(N, \mu, T, \omega)$ of the N-layer BP (where μ is the chemical potential of BP equal to the difference between the Fermi level and the first conduction subband [25]) are provided in the supplementary material. In what follows, we calculate the spectral heat flux defined as the HTC per unit photon energy (SHTC) and measured in the units of $\mathrm{W/(m^2K\ eV)}$. We also assume that $N = 3$, $\mu = 0.1\ \mathrm{eV}$ (or $n = 6.4 \times 10^{12} cm^{-2}$in agreement with the experimental data in Ref. [46]) and $d = 20\ \mathrm{nm}$, unless otherwise stated.

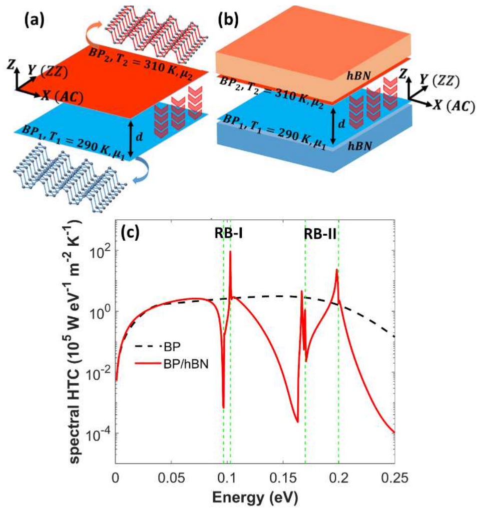

Fig. 1 A pair of parallel (a) BP and (b) BP/hBN plates separated by a vacuum gap of width d. The temperatures of the emitters and receivers are $T_2 = 310$ K and $T_1 = 290$ K. (c) SHTC for BP (dashed black curve) and BP/hBN (solid red curve) structures with $N = 3$, $\mu = 0.1$ eV, and $d = 20$ nm. Vertical dashed lines are the edges of the RBs of hBN.

Figure 1(c) compares the SHTC of the BP and BP/hBN parallel-plate structures. In agreement with the results of Ref. [23], the SHTC of BP (dashed black curve) reaches its peak of 3.1×10^5 at 0.146 eV. The proximity of this value to the Wien's frequency at 310 K ($\lambda_{\max} T_2 = 2898\ \mu$m K) indicates thermal occupation at this temperature. The solid red curve in Fig. 1(c) shows that the covering of the BP flakes with hBN films considerably enhances the SHTC at the upper edges of the RBs of hBN (i.e. at $\hbar\omega = 0.102$ and 0.198 eV), where hBN acts as an ENZ medium. The SHTC in the BP/hBN structure is also notably enhanced compared to the bare hBN structure (Fig. S2). Furthermore, as discussed in Fig. S3, the SHTC in the considered structure is higher than in the case of the graphene/hBN parallel-plate structure since $\mathrm{HTC_{BP}} > \mathrm{HTC_G}$.

To understand the origin of the enhanced NFRHT in the considered structures, we next analyze their energy transmission coefficients.

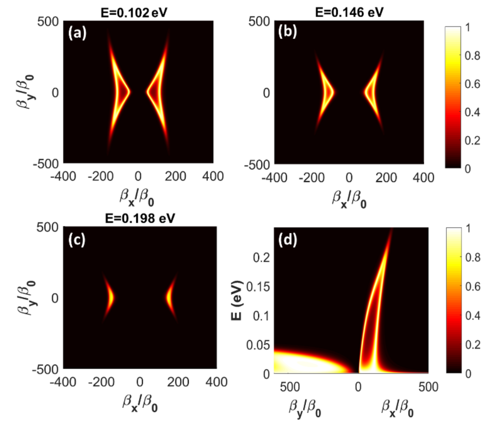

Fig. 2 Energy transmission coefficient $\xi(\hbar\omega, \beta_x, \beta_y)$ of BP parallel-plate structure for (a) $\hbar\omega = 0.102$ eV, (b) $\hbar\omega = 0.146$ eV, and (c) $\hbar\omega = 0.198$ eV. (d) spectra of energy transmission coefficient along the x and y axes. Regions with high values of ξ in this panel highlight the support of anisotropic SPPs by the BP parallel-plate structure.

Figures 2(a)-2(c) show the plots of $\xi(\omega, \beta_x, \beta_y)$ in the (β_x, β_y) plane for photons of three energies incident onto the BP parallel-plate structure. The emerging density plots, determined by the conductivity tensor components σ_{xx} and σ_{yy} [Figs. S4(a) and S4(b)], represent two branches of the coupled anisotropic SPPs of the BP flakes. Note that the strong anisotropic response of BP [i.e. $\sigma''_{yy} \gg \sigma''_{xx} > 0$] leads to the canalization of the coupled SPPs along the AC direction (x-axis). The two branches are clearly distinct at $\hbar\omega = 0.102$ eV [Fig. 2(a)] while they merge at $\hbar\omega = 0.198$ eV [Fig. 2(c)] indicating that the coupling is weakened by increasing the frequency, and that the wavenumbers region of non-negligible ξ is getting narrower. Moreover, the tunneling of the hybridized SPPs of the BP flakes leads to high values of the energy transmission coefficients that are recognized as the bright ($\xi = 1$) regions. The brightest region in Fig. 2(b) correspond to the maximum SHTC of the parallel-plate BP structure; i.e. to the dashed black curve in Fig. 1(c) at $\hbar\omega = 0.146$ eV. Figure 2(d) shows $\xi(\omega, \beta_x, 0)$ and $\xi(\omega, 0, \beta_y)$ of the coupled anisotropic SPPs, which are notably different due to the strong anisotropy of BP. It is also seen that the maximum value of $\xi(\omega, \beta_x, 0)$ is achieved over a broad range of frequencies and a narrow range of wave vectors, whereas the situation is reverse for $\xi(\omega, 0, \beta_y)$.

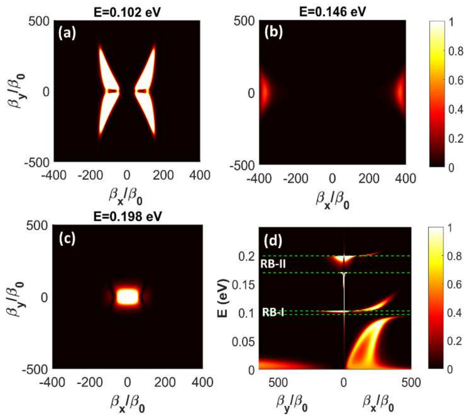

Fig. 3 Density plots of $\xi(\hbar\omega, \beta_x, \beta_y)$ for hBN-covered BP parallel-plate structure at (a) $\hbar\omega = 0.102\,\mathrm{eV}$, (b) $\hbar\omega = 0.146\,\mathrm{eV}$, and (c) $\hbar\omega = 0.198\,\mathrm{eV}$; horizontal dashed lines in (d) are the edges of the RBs of hBN and the high-ξ regions indicate the supported hybrid SPP-HPP modes.

It is known that the integration of an anisotropic 2D material with other functional materials, such as graphene [47] or hBN [48], modifies the supported modes. This is confirmed by Fig. 3(a) where the bright regions show that the hBN/BP parallel-plate structure supports hybrid modes of a modified topology and the corresponding ξ reaches its maximum over a broader area in the (β_x, β_y) plane for $\hbar\omega = 0.102\,\mathrm{eV}$, as compared to Fig. 2(a). Note that here topology refers to the trend of regions with high values of ξ. At this frequency, which almost coincides with the upper edge of the RB-I, hBN acts as an ENZ medium with $\varepsilon_z' = -0.2$ [see Figs. S4(c)]. The support of the hybrid SPP-HPP mode at the hBN's ENZ frequency leads to a more than 90-fold enhancement of the SHTC, which is represented by the first peak of the solid red curve in Fig. 1(c). The small values of ξ at $\hbar\omega = 0.146\,\mathrm{eV}$ [Fig. 3(b)] result in the negligible SHTCs in Fig. 1(c). Figure 3(c) shows the EFC of the hybrid SPP-HPP mode with energy 0.198 eV, which is close to the upper edge of RB-II and corresponds to $\varepsilon_x' = -0.18$. One can see that the noticeable modification of the mode topology [cf. Fig. 2(c)] leads to higher energy transmission coefficients. This explains the considerably high value of SHTC ($= 23.4 \times 10^5$) evidenced by the corresponding sharp peak of the solid red curve in Fig. 1(c).

In Fig. 3(d) we plot the energy transmission coefficient of the coupled SPP-HPP modes along the x and y axes. One can see that, outside the RBs, the modes predominantly have the anisotropic characteristics of the BP's SPPs, whereas inside the RB-II they inherit the isotropic features of the hBN's HPPs in the xy plane. It is also seen that the coupling of the HPPs of hBN to the SPPs of BP along the AC direction gives $\xi(\omega, 0, \beta_y)$ its maximum values around the upper edge of RB-I.

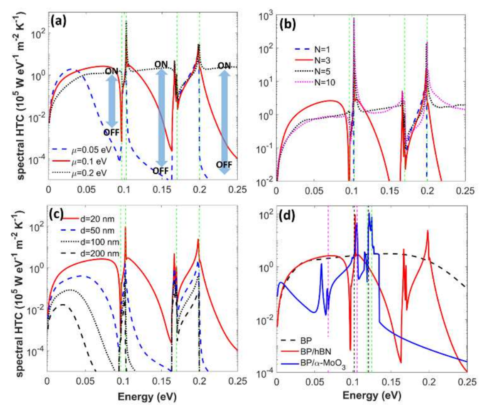

Fig. 4 SHTC of the BP/hBN parallel-plate structure for different values of (a) μ ($N = 3$, $d = 20\,\mathrm{nm}$), (b) N ($\mu = 0.1\,\mathrm{eV}$, $d = 20\,\mathrm{nm}$), and (c) d ($N = 3$, $\mu = 0.1\,\mathrm{eV}$). (d) compares the SHTCs of BP, BP/hBN, and BP/α-MoO_3 structures for $N = 3$, $\mu = 0.1\,\mathrm{eV}$ and $d = 20\,\mathrm{nm}$. The vertical dashed lines in (d) are the edges of the RBs of α-MoO_3 and the resonances of the SHTC for the BP/α-MoO_3 parallel-plates occur at the upper edges; i.e. the ENZ frequencies.

As the final point, we analyze how changing the parameters of BP (μ and N), altering the gap d between the plates, and replacing hBN with α-MoO_3 modify the NFRHT. The active tuning of the SHTC by varying the chemical potential of BP, which is practically achievable by gating [49], is illustrated by Fig. 4(a). It is seen that outside of the RBs, the NFRHT can be switched between the ON ($\mu = 0.2\,\mathrm{eV}$ or $n = 3.3 \times 10^{13} cm^{-2}$) and OFF ($\mu = 0.05\,\mathrm{eV}$ or $n = 1.3 \times 10^{12} cm^{-2}$) states indicated by the double-sided arrows. The ON/OFF functionality comes from the tunability of BP SPPs. In fact, outside of the RBs, the supported modes posses characteristics of SPPs of the BP parallel-plate structure that can be noticeably tuned by μ. This property leads to the tunability of the SHTC of the BP parallel-plate, as discussed in Ref. 23 and shown in Fig. S5(a), and consequently the active tuning of the BP/hBN parallel-plates' SHTC. This feature is also observed for the ENZ frequencies. It is also seen that the SHTC enhancement grows from 11.0×10^5 to 368.3×10^5 for $\hbar\omega = 0.102$ eV and from 15.5×10^5 to 30.6×10^5 for $\hbar\omega = 0.198$ eV when μ is increased from 0.05 to 0.2 eV.

It is known that the bandgap and, therefore, the optical properties of the BP thin films are passively tunable via the number of the layers [25]. Therefore, the same feature is expected to be observed for the SHTC. In agreement with the results of Ref. 23, Fig. S5(b) exhibits that at, $\mu = 0.1\ eV$, SHTC of the BP parallel-plates reaches saturated values for $N = 3$, then it decreases for the thicker BP films ($N > 3$). This behavior is different for the case of BP/hBN parallel-plates. As Fig. 4(b) illustrates, for this case the SHTC is seen to be relatively small for a single-layer BP (dashed blue curve) but steeply grow for $N = 3$ (solid red curve) and saturates at the ENZ frequencies close to the upper edges of the RBs for $N = 5$ (dotted black curve). Since efficient active tuning of the BP flakes is achievable for thicker films [49], dotted pink curve in Fig. 4(d) proves that it is still possible to obtain high values of the SHTC at the ENZ frequencies for thick BP films ($N = 10$). Note that we have investigated the SHTC for the other numbers of the BP layers, as well. However, for the sake of briefness, here the results for $N = 1, 3, 5$ and 10 are presented. Figure 4(c) also shows that increasing the gap between the parallel-plates reduces the efficiency of the NFRHT.

The NFRHT in the BP parallel-plate structure can be significantly modified by replacing hBN with another phononic material from the vdW family — α-MoO_3. The comparison of the three spectra in Fig. 4(d) shows that this replacement: (i) notably enhances the SHTC near the ENZ frequencies of α-MoO_3, once solid blue and dashed black curves are compared (see also the plots of the permittivities of α-MoO_3 along the x, y, and z directions in Fig. S6); (ii) spectrally modifies the SHTC resonances, as the solid blue and solid red curves are compared; and (iii) creates an additional resonance around $\hbar\omega_{\mathrm{LO},y}$ due to the in-plane anisotropy of α-MoO_3. Note that due to the in-plane and out-of-plane anisotropy of α-MoO_3, $\varepsilon_x \neq \varepsilon_y \neq \varepsilon_z$. This feature leads to the appearance of three resonances at the ENZ frequencies of α-MoO_3 (i.e. at $\hbar\omega_{\mathrm{LO},x} = 0.12051\ eV$, $\hbar\omega_{\mathrm{LO},y} = 0.10551\ eV$ and $\hbar\omega_{\mathrm{LO},z} = 0.12448\ eV$) at which ε_x, ε_y and ε_z obtain values close to zero, respectively. Moreover, the main purpose of this study is to investigate SHTC in parallel-plate heterostructures composed of BP and polar vdW materials (i.e. hBN and MoO_3). However, it is also possible to employ the other polar materials such as SiO_2 [15, 50], Al_2O_3 [16], and SiC [17, 18] to spectrally modify the SHTC. This point has been already proved in previous reports about graphene/SiO_2 [50] and graphene/SiC [51] parallel-plates. Consequently, for the sake of completeness of our discussion, we have investigated the SHTC in BP/SiC parallel-plate structure in Fig. S7. As expected, the SHTC is spectrally shifted however, the enhancement is not as strong as the BP/hBN case.

Summarizing, we have analyzed the NFRHT between two parallel non-rotated BP flakes due to the tunneling of the anisotropic SPPs supported by the flakes. It was shown that the covering of the BP flakes with hBN films leads to the hybridization of the BP's SPPs with the hBN's HPPs and to the significant enhancement of the NFRHT at the hBN's ENZ frequencies. We also demonstrated the possibility of actively switching between the ON and OFF states of the NFRHT by changing the chemical potential of the BP and the possibility of modifying the NFRHT *via* altering the number of the BP layers in the BP/hBN vdW parallel-plate structure. The replacement of hBN with α-MoO_3 showed the spectral and strong modification of the NFRHT in the BP/α-MoO_3 parallel-plate structure compared to the BP/hBN one. Our results suggest the high efficiency of the analyzed structures in the thermal management of optoelectronic devices.

See the supplementary material for details of the derivations, additional figures, and explanations.

TUBITAK (120E422); Russian Science Foundation (19-13-00332).

AUTHOR DECLARATIONS

Conflict of Interest

The authors declare no conflict of interest.

DATA AVAILABILITY

The data that support the findings of this study are available from the corresponding authors upon reasonable request.

REFERENCES

[1] D. Polder and M. Van Hove, "Theory of Radiative Heat Transfer between Closely Spaced Bodies", Phys. Rev. B 4, 3303 (1971).

[2] A. Narayanaswamy and G. Chen, "Surface modes for near field thermophotovoltaics", Appl. Phys. Lett. 82, 3544 (2003).

[3] A. Lenert, D. M. Bierman, Y. Nam, W. R. Chan, I. Celanovic, M. Soljacic, and E. N. Wang, "A nanophotonic solar thermophotovoltaic device", Nat. Nanotechnol. 9, 126 (2014).

[4] Z. M. Zhang, Nano/Microscale Heat Transfer (Springer Nature, Switzerland AG, 2020).

[5] C. Zhou, Y. Zhang, L. Qu, and H. Yi, "Near-field negative electroluminescent cooling via nanoparticle doping", J. Quant. Spectrosc. Radiat. Transfer 245, 106889 (2020).

[6] P. Ben-Abdallah and S.-A. Biehs, "Phase-change radiative thermal diode," Appl. Phys. Lett. 103 (19), 191907 (2013).

[7] P. Ben-Abdallah and S.-A. Biehs, "Near-Field Thermal Transistor", Phys. Rev. Lett. 112, 044301 (2014).

[8] D. Thompson, L. Zhu, R. Mittapally, S. Sadat, Z. Xing, P. McArdle, M. M. Qazilbash, P. Reddy & E. Meyhofer, "Hundred-fold enhancement in far-field radiative heat transfer over the blackbody limit", Nature 561, 216–221 (2018).

[9] P. Ben-Abdallah, K. Joulain, J. Drevillon, and G. Domingues, "Near-Field Heat Transfer Mediated by Surface Wave Hybridization Between Two Films," J. Appl. Phys. 106 (4), 044306 (2009).

[10] S. A. Biehs, P. Ben-Abdallah, F. S. S. Rosa, K. Joulain, and J. J. Greffet, "Nanoscale Heat Flux Between Nanoporous Materials," Opt. Express, 19 (S5), A1088–A1103 (2011).

[11] R. Guérout, J. Lussange, F. S. S. Rosa, J.-P. Hugonin, D. A. R. Dalvit, J.-J. Greffet, A. Lambrecht, and S. Reynaud, "Enhanced radiative heat transfer between nanostructured gold plates", Phys. Rev. B 85, 180301 (2012).

[12] P. Sabbaghi, L. Long, X. Ying, L. Lambert, S. Taylor, C. Messner, and L. Wang, "Super-Planckian radiative heat transfer between macroscale metallic surfaces due to near-field and thin-film effects", J. Appl. Phys. 128, 025305 (2020).

[13] V. Fernández-Hurtado, F. J. García-Vidal, Shanhui Fan, and J. C. Cuevas, "Enhancing Near-Field Radiative Heat Transfer with Si-based Metasurfaces", Phys. Rev. Lett. 118, 203901 (2017).

[14] J. DeSutter, L. Tang, and M. Francoeur, "A near-field radiative heat transfer device", Nat. Nanotechnol. 14, 751–755 (2019).

[15] M. Ghashami, H. Geng, T. Kim, N. Iacopino, S. K. Cho, and K. Park, "Precision Measurement of Phonon-Polaritonic Near-Field Energy Transfer between Macroscale Planar Structures Under Large Thermal Gradients", Phys. Rev. Lett. 120, 175901 (2018).

[16] R. S. Ottens, V. Quetschke, S. Wise, A. A. Alemi, R. Lundock, G. Mueller, D. H. Reitze, D. B. Tanner, and B. F. Whiting, "Near-Field Radiative Heat Transfer between Macroscopic Planar Surfaces" Phys. Rev. Lett. 107, 014301 (2011).

[17] M. Francoeur, M. P. Mengüç, and R. Vaillon, "Near-field radiative heat transfer enhancement via surface phonon polaritons coupling in thin films", Appl. Phys. Lett. 93, 043109 (2008).

[18] L. Tang, J. DeSutter, and M. Francoeur, "Near-Field Radiative Heat Transfer between Dissimilar Materials Mediated by Coupled Surface Phonon- and Plasmon-Polaritons", ACS Photonics 7, 1304−1311 (2020).

[19] O. Ilic, M. Jablan, J. D. Joannopoulos, I. Celanovic, H. Buljan, and M. Soljačić, "Near-field thermal radiation transfer controlled by plasmons in graphene", Phys. Rev. B 85, 155422, (2012).

[20] J. Jiang and J. Wang, "Caroli formalism in near-field heat transfer between parallel graphene sheets", Phys. Rev. B 96, 155437 (2017).

[21] J. Yang, W. Du, Y. Su, Y. Fu, S. Gong, S. He, and Y. Ma, "Observing of the Super-Planckian Near-Field Thermal Radiation Between Graphene Sheets," Nat. Commun. 9, 4033 (2018).

[22] Y. Zhang, C. Zhou, L. Qu, and H. Yi, "Active control of near-field radiative heat transfer through nonreciprocal graphene surface plasmons", Appl. Phys. Lett. 116, 151101 (2020).

[23] Y. Zhang, H. Yi, and H. Tan, "Near-Field Radiative Heat Transfer between Black Phosphorus Sheets via Anisotropic Surface Plasmon Polaritons", ACS Photonics 5, 3739−3747 (2018).

[24] J. Shen, S. Guo, X. Liu, B. Liu, W. Wu, and H. He "Super-Planckian thermal radiation enabled by coupled quasi-elliptic 2D black phosphorus plasmons", Appl. Therm. Eng. 144, 403–410 (2018).

[25] T. Low, A. S. Rodin, A. Carvalho, Y. Jiang, H. Wang, F. Xia, and A. H. Castro Neto, "Tunable optical properties of multilayer black phosphorus thin films", Phys. Rev. B 90, 075434 (2014).

[26] T. Low, R. Roldan, H. Wang, F. Xia, P. Avouris, L. Martin Moreno, and F. Guinea, "Plasmons and Screening in Monolayer and Multilayer Black Phosphorus", Phys. Rev. Lett. 113, 106802 (2014).

[27] G. Qin, X. Zhang, S. Yue, Z. Qin, H. Wang, Y. Han, and M. Hu "Resonant bonding driven giant phonon anharmonicity and low thermal conductivity of phosphorene", Phys. Rev. B 94, 165445 (2016).

[28] S. A. Biehs, F. S. S. Rosa, and P. Ben-Abdallah, "Modulation of Near-Field Heat Transfer Between Two Gratings," Appl. Phys. Lett. 98 (24), 243102 (2011).

[29] S.-A. Biehs, M. Tschikin, and P. Ben-Abdallah, "Hyperbolic Metamaterials as an Analog of a Blackbody in the Near Field" Phys. Rev. Lett. 109, 104301 (2012).

[30] S. Molesky, C. J. Dewalt, and Z. Jacob, "High temperature epsilon-near-zero and epsilon-near-pole metamaterial emitters for thermophotovoltaics", Opt. Express 21, A96-A110 (2013).

[31] S. A. Biehs, M. Tschikin, R. Messina, and P. Ben-Abdallah, "Super-Planckian Near-Field Thermal Emission with Phonon-

Polaritonic Hyperbolic Metamaterials," Appl. Phys. Lett. 102 (13), 131106 (2013).

[32] M. Lim, J. Song, S. S. Lee, and B. J. Lee, "Tailoring Near-Field Thermal Radiation Between Metallo-Dielectric Multilayers Using Coupled Surface Plasmon Polaritons," Nat. Commun., 9, 4302 (2018).

[33] X. L. Liu and Z. M. Zhang, "Giant enhancement of nanoscale thermal radiation based on hyperbolic graphene plasmons", Appl. Phys. Lett. 107, 143114 (2015).

[34] C. Zhou, X. Wu, Y. Zhang, H. Yi, and M. Antezza, "Polariton topological transition effects on radiative heat transfer", Phys. Rev. B 103, 155404 (2021).

[35] M. He, H. Qi, Y. Ren, Y. Zhao, Y. Zhang, J. Shen, and M. Antezza "Radiative thermal switch driven by anisotropic black phosphorus plasmons", Opt. Express 28, 26922 (2020).

[36] X. L. Liu and Y. M. Xuan, "Super-Planckian Thermal Radiation Enabled by Hyperbolic Surface Phonon Polaritons," Sci. China Technol. Sci. 59 (11), 1680–1686 (2016).

[37] X. L. Liu, J. D. Shen, and Y. M. Xuan, "Pattern-Free Thermal Modulator Via Thermal Radiation Between Van Der Waals Materials," J. Quant. Spectrosc. Radiat. Transfer 200, 100–107 (2017).

[38] K. Tielrooij, N. C. H. Hesp, A. Principi et al., "Out-of-plane heat transfer in van der Waals stacks through electron–hyperbolic phonon coupling" Nat. Nanotechnol. 13, 41–46 (2018).

[39] Z. B. Zheng, N. S. Xu, S. L. Oscurato, M. Tamagnone, F. S. Sun, Y. Z. Jiang, Y. L. Ke, J. N. Chen, W. C. Huang, W. L. Wilson, A. Ambrosio, S. Z. Deng, and H. J. Chen, "A Mid-Infrared Biaxial Hyperbolic Van Der Waals Crystal," Sci. Adv., 5(5), p. eaav8690 (2019).

[40] X. Wu, C.Fu, and Z. M. Zhang, "Near-Field Radiative Heat Transfer Between Two a-MoO_3 Biaxial Crystals", J. Heat Transfer. Jul 142 (7), 072802-1-10 (2020).

[41] X. H. Wu, C. J. Fu, and Z. M. Zhang, "Influence of hBN Orientation on the Near-Field Radiative Heat Transfer Between Graphene/hBN Heterostructures," J. Photon. Energy 9 (3), 1 (2018).

[42] B. Zhao, B. Guizal, Z. M. Zhang, S. Fan, and M. Antezza "Near-field heat transfer between graphene/hBN multilayers", Phys. Rev. B 95, 245437 (2017).

[43] K. Shi, F. Bao, and S. He, "Enhanced Near-Field Thermal Radiation Based on Multilayer Graphene-hBN Heterostructures", ACS Photonics 4, 971 (2017).

[44] B. Song, A. Fiorino, E. Meyhofer, and P. Reddy, "Near-field radiative thermal transport: From theory to experiment", AIP Adv. 5, 053503 (2015).

[45] O. V. Kotov and Yu. E. Lozovik, "Hyperbolic hybrid waves and optical topological transitions in few-layer anisotropic metasurfaces", Phys. Rev. B 100, 165424 (2019).

[46] S. Biswas, W. S. Whitney, M. Y. Grajower, K. Watanabe, T. Taniguchi, H. A. Bechtel, G. R. Rossman, and H. A. Atwater, "Tunable intraband optical conductivity and polarization-dependent epsilon-near-zero behavior in black phosphorus", Sci. Adv. 7, eabd4623 (2021).

[47] H. Hajian, I. D. Rukhlenko, G. Hanson, and E. Ozbay, "Hybrid surface plasmon polaritons in graphene coupled anisotropic van der Waals material waveguides", J. Phys. D: Appl. Phys. 54, 455102 (2021).

[48] H. Hajian, I. D. Rukhlenko, G. Hanson, T. Low, and E. Ozbay, "Tunable plasmon-phonon polaritons in anisotropic 2D materials on hexagonal boron nitride", Nanophotonics 9, 3909 (2020).

[49] B. Deng, V. Tran, Y. Xie, H. Jiang, C. Li, Q. Guo, X. Wang, H. Tian, S. J. Koester, H. Wang, J. J. Cha, Q. Xia, L. Yang & F. Xia, "Efficient electrical control of thin-film black phosphorus bandgap", Nat. Commun. 8, 14474 (2017).

[50] X. L. Liu and Z. M. Zhang, "Graphene-assisted near-field radiative heat transfer between corrugated polar materials", Appl. Phys. Lett. 104, 251911 (2014).

[51] M. He, H. Qi, Y. Ren, Y. Zhao, and M. Antezza, "Active control of near-field radiative heat transfer by a graphene-gratings coating-twisting method", Opt. Lett. 45, 2914-2917 (2020).

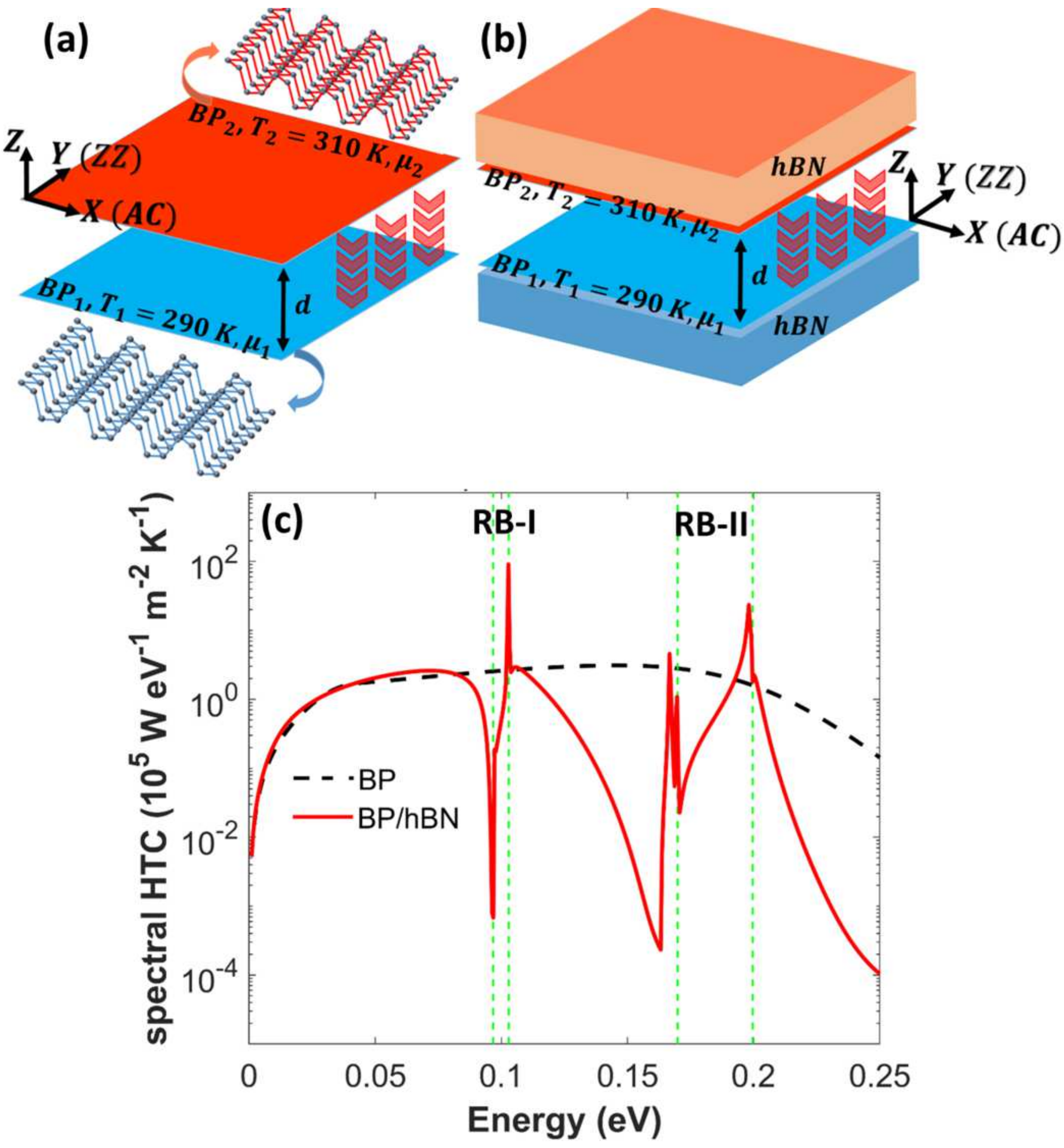
(a)
(b)
$BP_2, T_2 = 310\ K, \mu_2$
$BP_1, T_1 = 290\ K, \mu_1$
Z
$Y\ (ZZ)$
$X\ (AC)$
d
hBN
hBN
(c)
RB-I
RB-II
BP
BP/hBN
spectral HTC (10^5 W eV^{-1} m^{-2} K^{-1})
Energy (eV)
10^2
10^0
10^{-2}
10^{-4}
0
0.05
0.1
0.15
0.2
0.25

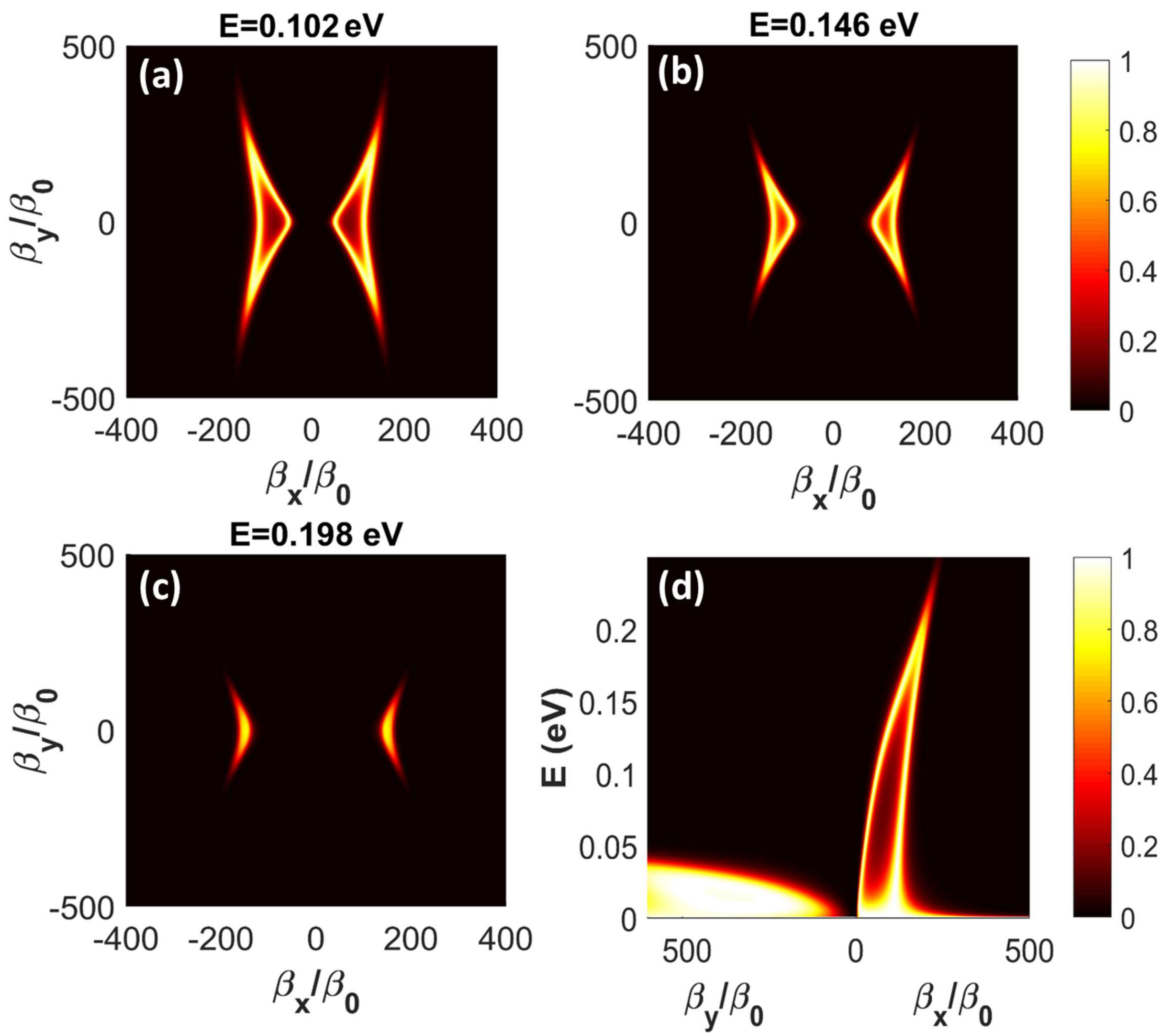
E=0.102 eV
(a)
E=0.146 eV
(b)
E=0.198 eV
(c)
(d)
β_y/β_0
β_x/β_0
E (eV)
500
0
-500
-400
-200
0
200
400
0.2
0.15
0.1
0.05
1
0.8
0.6
0.4
0.2

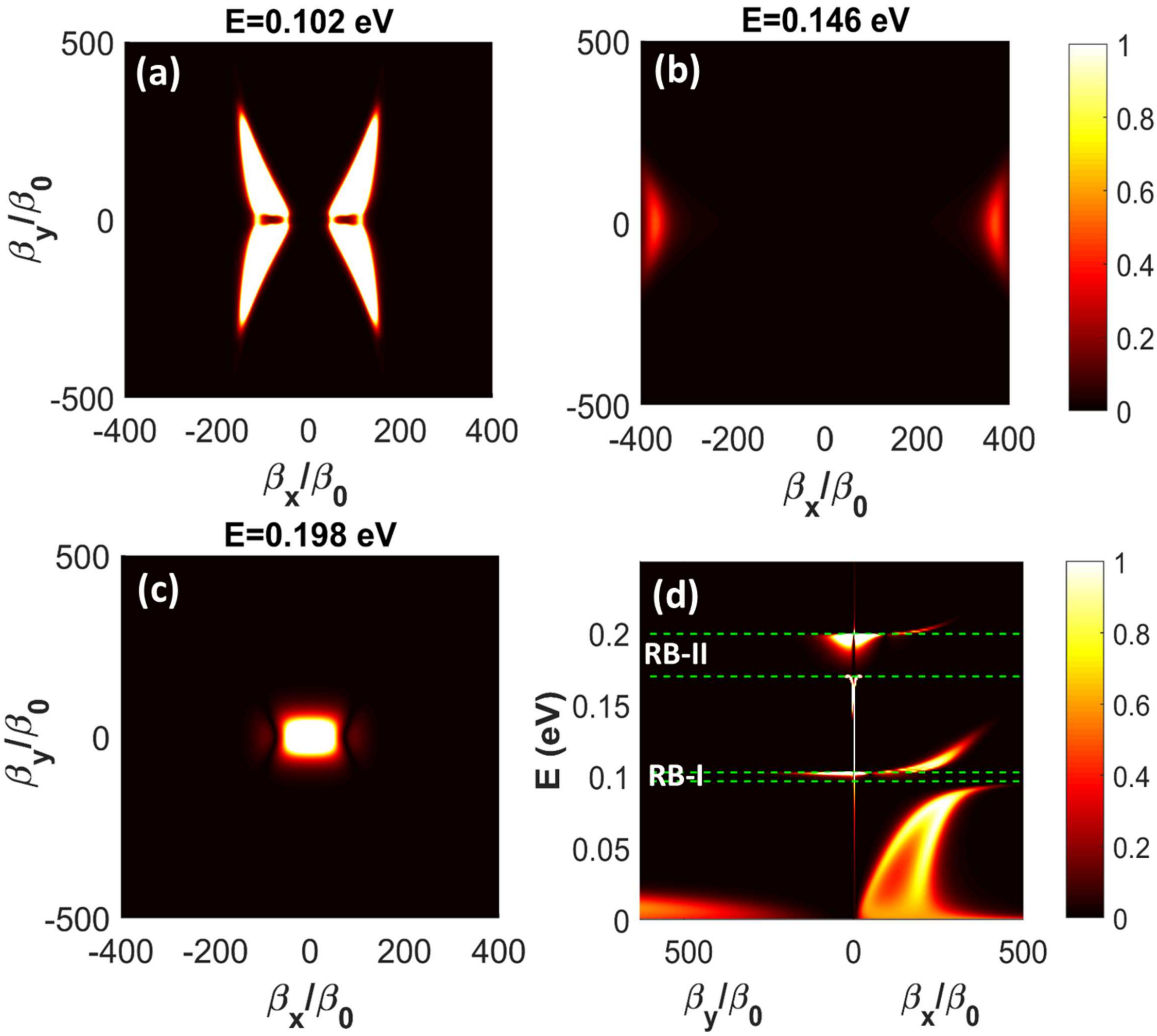
E=0.102 eV
(a)
E=0.146 eV
(b)
E=0.198 eV
(c)
(d)
RB-II
RB-I
E (eV)
β_y/β_0
β_x/β_0

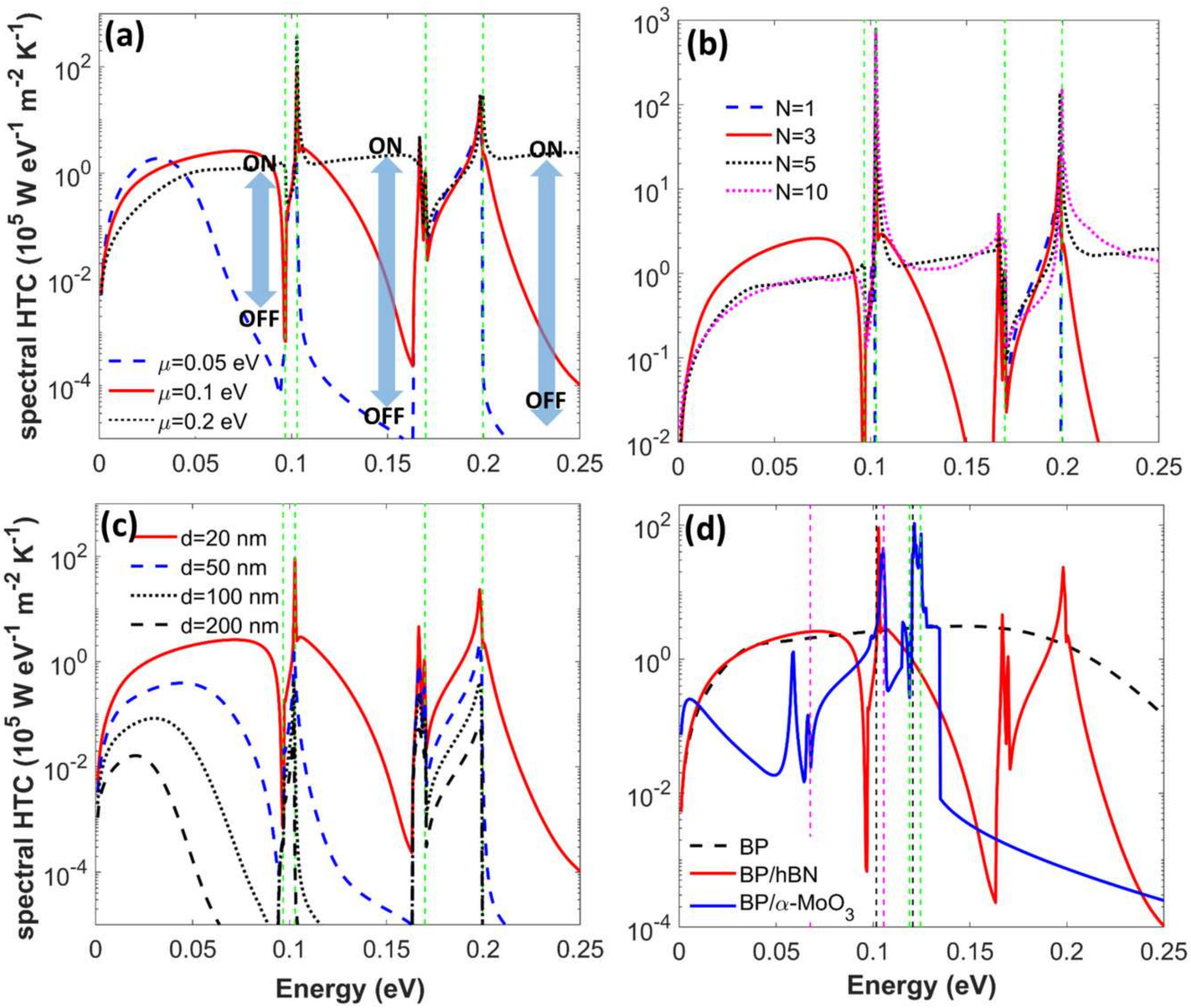
(a)
(b)
(c)
(d)
spectral HTC (10^5 W eV^{-1} m^{-2} K^{-1})
Energy (eV)
ON
OFF
μ=0.05 eV
μ=0.1 eV
μ=0.2 eV
N=1
N=3
N=5
N=10
d=20 nm
d=50 nm
d=100 nm
d=200 nm
BP
BP/hBN
BP/α-MoO$_3$